Materials Science & Engineering C 101 (2019) 232–242

Contents lists available at ScienceDirect

Materials Science & Engineering C

journal homepage: www.elsevier.com/locate/msec

Tantalum nanoparticles reinforced polyetheretherketone shows enhanced bone formation

Hao Zhu[a,b], Xiongfa Ji[a], Hanfeng Guan[a], Liming Zhao[a], Libo Zhao[a], Changyu Liu[a], Cong Cai[a], Weijing Li[a], Tenghui Tao[a], Janne Elin Reseland[b], Håvard Jostein Haugen[b,*], Jun Xiao[a,*]

[a] Department of Orthopedic Surgery, Tongji Hospital, Tongji Medical College, Huazhong University of Science and Technology, 1095 Jiefang Avenue, Wuhan 430030, China

[b] Department of Biomaterials, Institute of Clinical Dentistry, Faculty of Dentistry, University of Oslo, P.O. Box 1109, Blindern, NO-0317 Oslo, Norway

ARTICLE INFO

Keywords:
Polyetheretherketone
Tantalum
Elastic modulus
Osseointegration
In vivo

ABSTRACT

Polyetheretherketone (PEEK) has been used in orthopedic surgery for several decades. Numerous methods were invented to alter the properties of PEEK. By adding nanoparticles, fibers, *etc.*, elastic modulus and strength of PEEK can be changed to meet certain demand. In this study, tantalum (Ta), a promising metal, was introduced to modify the properties of PEEK, in which PEEK was reinforced with different contents of tantalum nanoparticles (from 1 wt% to 9 wt%). Mechanical properties and biological functions (both *in vitro* and *in vivo*) were then investigated. The highest elastic modulus and compressive strength were observed in 3%Ta-PEEK. Cell experiments as cell adhesion, collagen secretion, biomineralization and osteogenesis related gene expression showed preferable results in 3%Ta-PEEK and 5%Ta-PEEK. Improved bone integration was shown in 3%Ta-PEEK and 5%Ta-PEEK *in vivo*. Above all, enhanced mechanical properties and promoted bone formation were proved for 3%Ta-PEEK and 5%Ta-PEEK compared to others groups both *in vitro* and *in vivo*, suggesting that the addition of tantalum nanoparticles modified the osseointegration ability of PEEK. This composite of tantalum and PEEK could have a clinical potential for orthopedic implants.

1. Introduction

Orthopedic materials have for a long time been in focus in research. As an ideal orthopedic material for implant fabrication, many properties should be included. Biocompatibility should with no doubt be first taken into consideration, while osteogenesis related properties such as osteoguiding, osseointegration, and bone ingrowth are also of great significance [1,2]. Metals and alloys of medical grades were introduced into this area from the very beginning due to their high performance and are widely used for clinical implants nowadays, for example, titanium and its alloys are frequently chosen as the materials for orthopedic and dental implants [3,4]. Although high strength, favorable wear performance, good formability and low toxicity are all preferable properties that metals can provide [3], notable disadvantages still exist, *e.g.*, high elastic modulus, artifacts in X-ray, limitation in magnetic resonance imaging, potential metal ion release and subsequent osteolysis or allergenicity, which cannot be neglected in clinical occasions [6,7]. Most importantly, the stress shielding effect caused by high elastic modulus is always a potential risk for metal implants, especially when used in load-bearing areas such as the femoral component of hip replacement [2,5].

Tantalum (Ta) has been used for implants both for orthopedics and dentistry [2,6]. This metal has an outer layer of tantalum oxide which can provide excellent anti-corrosion property [6]. Tantalum could be formed with a highly porous structure that could mimic the cancellous bone [7,8]. Bone ingrowth was proved to be strong in tantalum cup and augment which were clinically used in hip replacement and revision [9–11]. On the other hand, tantalum could be applied in a nanoparticle form, which also showed preferable biocompatibility and osteogenic properties [12–14].

Compared to metals, polymers present particularly lower modulus. Nowadays polymers are widely used in various biomedical applications, one of which is the polyetheretherketone (PEEK). As a semi-crystalline linear polycyclic aromatic thermoplastic, PEEK was already commercialized for industrial applications in extreme conditions, such as aircraft and turbine blades. Due to its high performance, PEEK was a potential candidate for replacing metal implant component in the late 1990s [15]. The high inertia of this polymer also makes it very stable

* Corresponding authors.
E-mail addresses: zhuhao_92@hust.edu.cn (H. Zhu), jixiongfa@hust.edu.cn (X. Ji), hguan@hust.edu.cn (H. Guan), zhaoliming@hust.edu.cn (L. Zhao), taotenghui@hust.edu.cn (T. Tao), j.e.reseland@odont.uio.no (J.E. Reseland), h.j.haugen@odont.uio.no (H.J. Haugen), jun_xiao@hust.edu.cn (J. Xiao).

https://doi.org/10.1016/j.msec.2019.03.091
Received 23 July 2018; Received in revised form 23 March 2019; Accepted 24 March 2019
Available online 27 March 2019

almost in all solvents at room temperature [16]. PEEK also presents better biocompatibility and immunoreactions with bone tissues or even other tissues compared to other polymers [17–19]. One of the successful applications of PEEK in bone surgery is the cage for vertebrate fusion [15,20].

Since PEEK is a high inert material, numerous methods were invented to reinforce the properties and enhance the bioactivity of PEEK. By adding nanoparticles, fibers, *etc.*, elastic modulus and strength of PEEK can be optimized to meet certain demand [21]. Carbon fibers, glass fibers, hydroxyapatite particles, titanium dioxide were all confirmed the quality of reinforcing the mechanical performance of PEEK, while at the same time showed high compatibility with the bone tissues [22–27]. Coatings were also utilized to modified interface between bone tissues and PEEK. Tao Lu et al. coated Ta_2O_5 on the surface of PEEK using plasma immersion ion implantation. It was demonstrated that this combination could promote osteogenesis [28]. Enhanced osseointegration was also found by plasma-spraying hydroxyapatite on carbon fiber reinforced PEEK [29]. Nevertheless, there is still a potential risk of disbonding for coatings. On the other hand, reinforced PEEK was also proved with high wear performance, showing high potential as a material for artificial joints [30–33]. Since tantalum nanoparticles are stable and biocompatible, they could be used as reinforcement particles for PEEK, and potentially alter the properties of PEEK for better prospect in orthopedic use.

The aim of the study was to combine the advantages of tantalum and PEEK by adding tantalum nanoparticles to PEEK in order to increase both the mechanical properties and bioactivity, providing a potential new composite biomaterial for orthopedic use. Multiple compositions of tantalum nanoparticles reinforced polyetheretherketone (Ta-PEEK) materials (weight ratio of tantalum ranging from 1% to 9%, namely 1%Ta-PEEK, 3%Ta-PEEK, 5%Ta-PEEK, 7%Ta-PEEK and 9%Ta-PEEK) were fabricated. We examined the mechanical properties as well as the biological features of Ta-PEEK by *in vitro* studies on MC3T3-E1 cells and *in vivo* test on Sprague Dawley rats.

2. Materials and methods

2.1. Sample fabrication and preparation

Polyetheretherketone powder (Victrex, biomedical grade, D50 = 200 μm, UK) was fully commixed with tantalum nanoparticles (Beijing Dk Nano technology Co., LTD, China) using ball-milling machine (WZM ball-milling machine, Yixing Haoqiang industry, China). The ball milling was performed using aluminum oxide balls and nylon jars. Ball-to-powder ratio was set as 1:1 and rotating speed was set at 100 r/min in which the impacting sound was loudest. Rotation direction was inverted every 6 h and total milling time lasted for 24 h. The weight ratios of tantalum nanoparticles were controlled at 1%, 3%, 5%, 7% and 9%, and the corresponding volume ratios were 0.08 vol%, 0.24 vol%, 0.41 vol%, 0.58 vol%, and 0.76 vol% respectively. Pure PEEK powder was set as the control group. For each group, heat-compressing molding was utilized to form the material according to certain procedures [34]. Briefly, the mixed powder was first dried in 85 °C for 6 h and then put in the mold and heated at a rate of 10 °C per minute. The maximum temperature was set at 340 °C. The pressure was held at 5 MPa from the start until the temperature of the mixture increased to 320 °C, afterward the pressure was raised to 15 MPa for the rest heating cycle. The mixture was held at 340 °C for 8 min and then cooled down to 100 °C in a mold.

After molding, samples were then cut into several sizes for experimental use. Small square samples (10 mm × 10 mm × 1 mm) were used for surface characterization and *in vitro* studies in 24-well culture plates. Big square samples (20 mm × 20 mm × 1 mm) were used in the RNA expression related tests. Cylindrical samples with two different sizes (diameter 2 mm, length 10 mm and 12 mm) were used in the *in vivo* experiment (Fig. 1A and B). Cylindrical sample I was used for micro-computer tomography and histological analysis while cylindrical sample II was specially designed for pull-out test with an addition part for fixing. All the samples were washed with acetone, ethanol and deionized water successively in the ultrasonic washing machine for two times in order to remove the debris and cream on the samples. All samples were then rinsed with phosphate buffer saline (PBS) for three times and autoclaved before use.

2.2. Material properties

2.2.1. Surface morphology

The surface morphology was examined by scanning electron microscope (SEM, Hitachi S-3400N, Hitachi High-Technologies Europe GmbH, Germany) after sputtered with 5 nm of platinum coating (Gressington 308R, Cressington Scientific Instruments, UK). The acceleration voltage was set at 15 kV and images were taken in different magnifications, with the energy-dispersive X-ray spectroscopy (EDS) performed afterward. Topographical parameters were acquired by analyzing the sample surfaces using blue laser profilometer (Sensofar Plμ 2300, Terrassa, Spain) with a 150× DI Nikon objective lens. Surface parameters as S_a, S_{ci}, S_{sk}, S_{ku} were chosen and calculated in SensoMap software (SensoMap Plus 4.1, Sensofar, Terrassa, Spain).

2.2.2. Contact angle

The experiment was performed with contact angle measurement (OCA Plus 15, DataPhysics Instruments GmbH, Filderstadt, Germany) using the sessile drop mode with Laplace-Young model fitting. The measurement was performed with deionized water at 20 °C. An average of five consecutive measurements with a 3 μL drop at rate of 1 μL/s were performed. Five samples from each group were measured and the average was obtained.

2.2.3. Mechanical test

Compressive strength and Young's modulus were obtained and calculated following the ASTM standard. Electromechanical testing machine (3300 Floor Model Universal Testing Systems, Instron, USA) was applied for biomechanical test and eight specimens were tested for each group.

2.2.4. Thermogravimetric analysis and differential scanning calorimeter

The thermal properties of the composites were evaluated using thermogravimetric analysis (TGA) and differential scanning calorimeter (DSC). TGA tests were run in air with the temperature rising from 30 °C to 900 °C at a speed of 10 K/min (TGA8000, PerkinElmer, USA). DSC was performed at the speed of 10 K/min where heating and cooling curves were both obtained (DSC 214 Polyma, Netzsch Gerätebau, Selb, Germany). Selected parameters as glass transition temperature (T_g), delta capacity (ΔCp), melting temperature (T_m), crystallization temperature (T_c), melting enthalpy (H_m), and degree of crystallinity (X_c) with a standard value of 130 J/g were calculated as previously reported [35].

2.3. In vitro studies

2.3.1. Cell culturing

MC3T3-E1 cell line (DSMZ, Braunschweig, Germany) was used to conduct the *in vitro* study. The cells were cultured in α-MEM essential medium (Gibco, USA) with 10% fetal bovine serum and 1% antibiotics (50 IU penicillin/ml and 50 μg streptomycin/ml) for expansion. Standard culturing environment as 37 °C humidified atmospheres with 5% CO_2 was utilized. The medium was changed every 3 days and cells were passaged when the coverage reached 90%. Osteogenic medium (100 nM dexamethasone, 10 mM beta-glycerol phosphate, and 50 μg/mL ascorbic acid) was used for 7 days, 14 days, and 21 days of experiments including alkaline phosphatase (ALP) activity, mineralization, collagen secretion and gene expression.

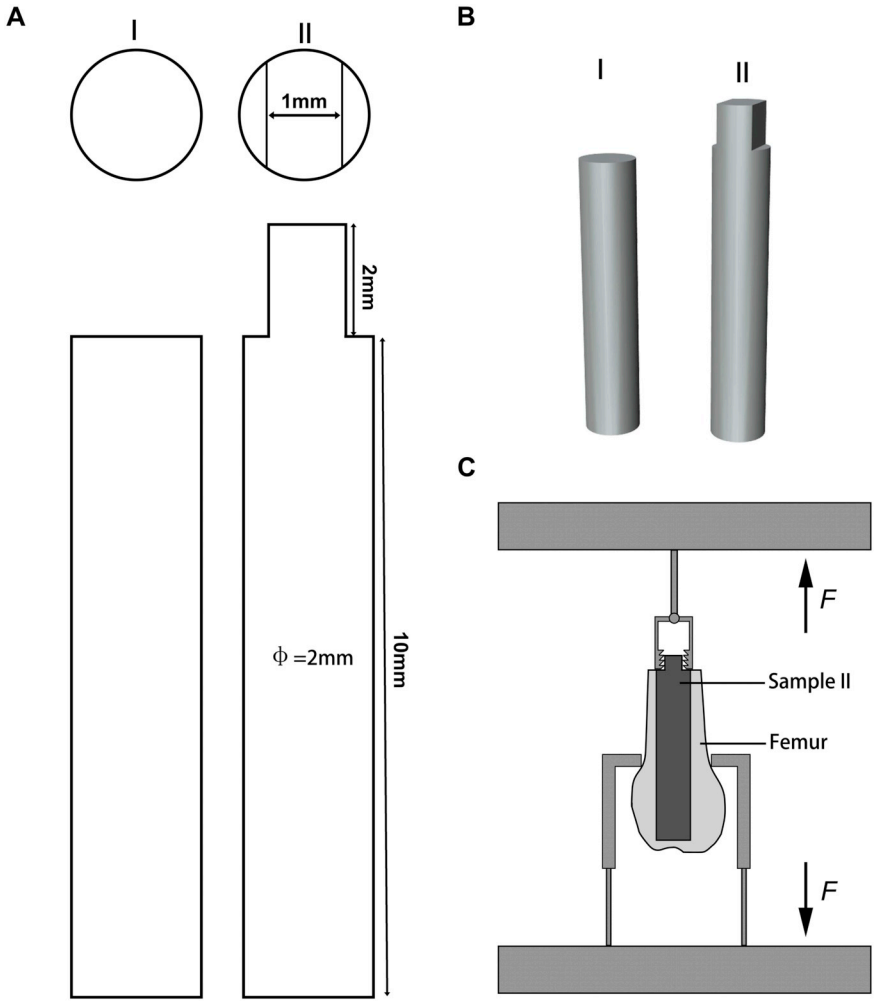

Fig. 1. Illustration of the cylindrical samples and pull-out test. (A) Top and front view of cylindrical sample I and II. (B) 3D model of the cylindrical samples. (C) Illustration of pull-out test on the rat femur.

2.3.2. Cell adhesion

MC3T3-E1 cells were seeded onto the surface of the samples ($10 \times 10 \times 1\ mm^3$) at a density of 5×10^3/well. After culturing for 24 and 48 h respectively, the medium was removed and samples were rinsed with PBS for 3 times, followed by the fixation with 4% paraformaldehyde in PBS. Samples were then stained with phalloidin and DAPI. Images were taken under confocal scanning microscopy (Leica TCS SPE Microsystems Wetzlar GmbH, Wetzlar, Germany).

2.3.3. Cell toxicity

The lactate dehydrogenase (LDH) activity in the culture medium was chosen as an indicator of cell toxicity. The activity of LDH was estimated according to the manufacturer's instructions (Roche Diagnostics, Mannheim, Germany). All the results were first removed of the background which was the absorbance of the culture medium without cells. Then the results from all the samples were presented relatively compared to the LDH activity in the medium of cells treated with PBS (low control, 0% of cell death) and of cells treated with 1% Triton X-100 (high control, 100% cell death). The cytotoxicity was calculated using the equation Eq. (1)

$$\text{Cytotoxicity}\ (\%) = (\text{experiment value} - \text{low control}) / (\text{high control} - \text{low control}) \times 100\% \quad (1)$$

2.3.4. Alkaline phosphatase activity

ALP activity was tested on 7 days, 14 days and 21 days after cell seeding, with the ALP activity kit (Nanjingjiancheng, China), following the manufacturer's protocol. After incubation, OD value at 405 nm was obtained. The ALP levels were normalized to the total protein content and results were described as μM/μg total proteins.

2.3.5. Collagen secretion

MC3T3-E1 cells were seeded onto the surface of the samples ($10 \times 10 \times 1\ mm^3$) at a density of 5×10^3/well. After 7 days and 14 days, the medium was removed and samples were rinsed with PBS for 3 times, followed by the fixation with 4% paraformaldehyde. Samples were then stained with 0.1% Sirius red (Sigma-Aldrich, St. Louis, USA) solution in picric acid for 18 h. After washed with 0.1 M acetic acid for three times, images were taken under the light microscope (Leica DMRBE, Germany). The staining was then eluted in a basal solution (0.2 M NaOH/methanol = 1:1) and OD value was read at 540 nm.

2.3.6. Mineralization

MC3T3-E1 cells were seeded onto the surface of the samples ($10 \times 10 \times 1\ mm^3$) at a density of 5×10^3/well. The medium was changed every three days. After culturing for 14 days and 21 days, the medium was removed and samples were rinsed with PBS for 3 times, followed by the fixation with 4% paraformaldehyde. Alizarin red (Sigma-Aldrich, St. Louis, USA) was used to quantify the calcification of the samples. The staining solution was prepared by dissolving Alizarin red in deionized water (40 mM) and adjusting the pH to 4.2. After

Table 1
Osteogenesis-related genes and primers.

Genes	Forward primer	Reverse primer
ALP	CAGCGGGTAGGAAGCAGTTTC	CCCTGCACCTCATCCCTGA
COL-1	GCCTCCCAGAACATCACCTA	GCAGGGACTTCTTGAGGTTG
OCN	GGTGCAGACCTAGCAGACACCA	AGGTAGCGCCGGAGTCTATTCA
OPN	CCAAGCGTGGAAACACACAGCC	GGCTTTGGAACTCGCCTGACTG
RUNX2	CCATAACGGTCTTCACAAATCCT	TCTGTCTGTGCCTTCTTGGTTC
β-Actin	CACCCGCGAGTACAACCTTC	CCCATACCCACCATCACACC

stained for 5 min, samples were rinsed with deionized water for three times and images were taken under the light microscope (Leica DMRBE, Germany). The staining was then eluted in 10% cetylpyridinium chloride in 10 mM sodium phosphate (pH = 7.0). The OD value was obtained at 565 nm.

2.3.7. Osteogenesis related gene expression

The expression of osteogenesis-related genes was analyzed by real-time polymerase chain reaction (qPCR). Five osteogenesis-related genes, namely, alkaline phosphatase (ALP), type-1 collagen (COL-1), osteocalcin (OCN), and osteopontin (OPN), runt-related transcription factor 2 (RUNX2), were selected (Table 1). Briefly, MC3T3-E1 cells were seeded onto the surface of the samples (20×20 x $1mm^3$) at a density of 2×10^4/well and cultured for 7 days, 14 days and 21 days subsequently. Cells on the surface were lysed using Trizol reagent (Invitrogen, USA) and RNA was extracted. The concentration of RNA was detected using nanodrop, after which the reverse transcription using the Superscript II first-strand cDNA synthesis kit (Thermo, Waltham, USA) was performed. The qPCR mix was prepared using the Trans Start Top Green qPCR SuperMix (Transgen Beijing, China) and experiment was carried with a thermocycler (Bio-rad thermocycler, Bio-rad, US).

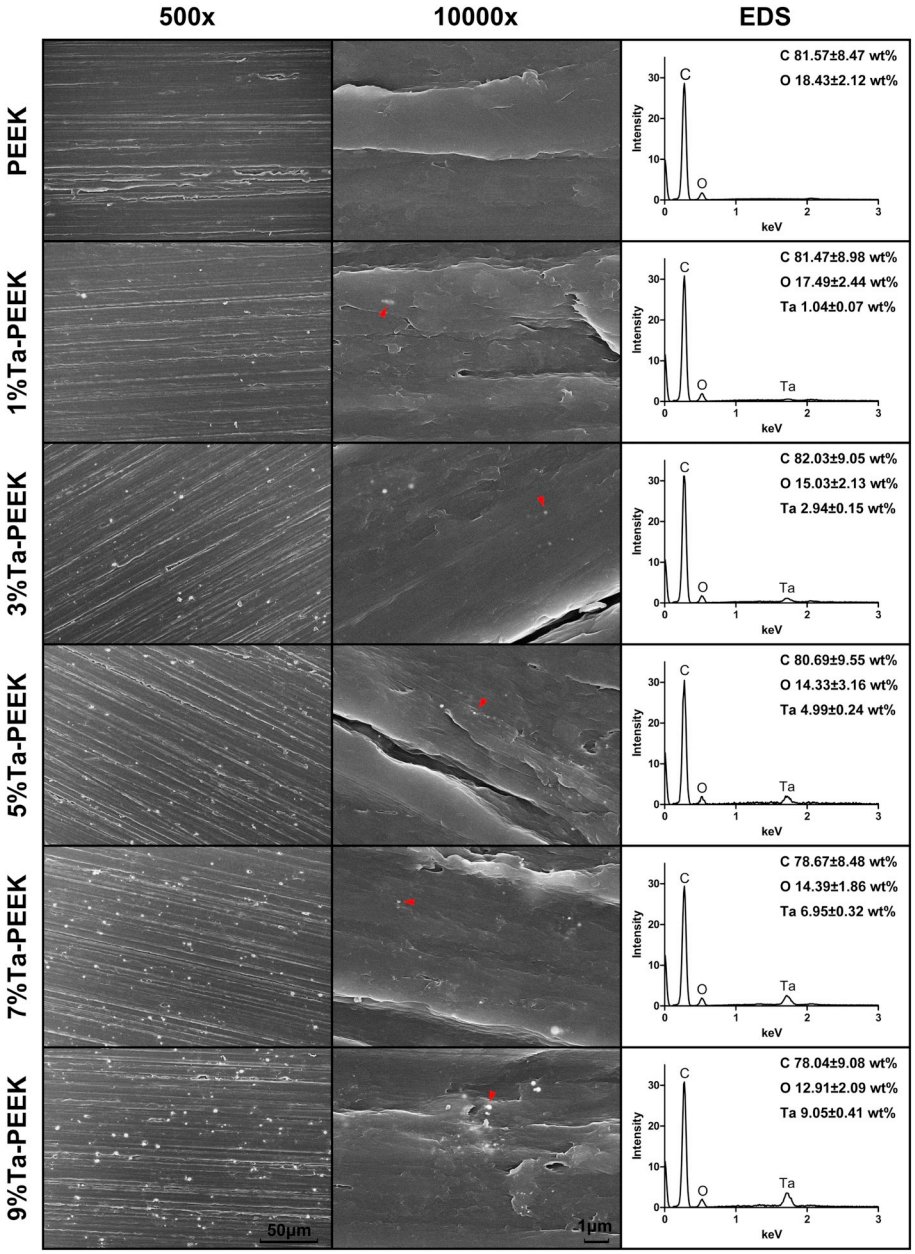

Fig. 2. SEM images of samples and EDS results. Red arrows referred to the tantalum particles. (For interpretation of the references to colour in this figure legend, the reader is referred to the web version of this article.)

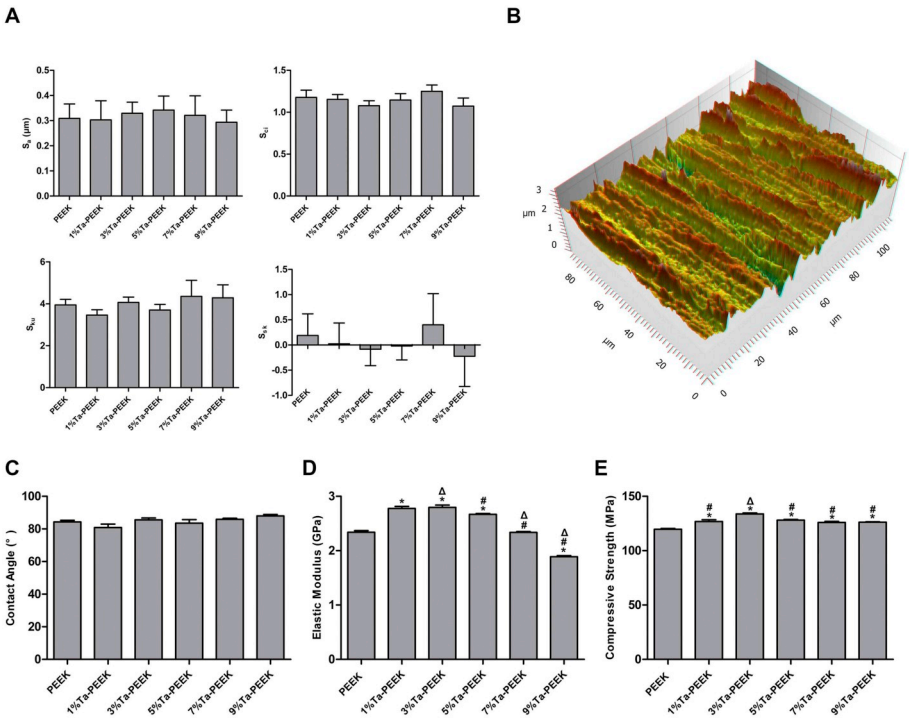

Fig. 3. Surface morphology and mechanical properties of the samples. (A) Surface parameters analyzed by a profilometer. No significant difference was found among the groups ($p > 0.05$). (B) The typical image of a 3D model of the sample surface. (C) Contact angles of the samples shown as mean ± SD. No significance was found among the groups ($p > 0.05$). (D) Elastic modulus. (E) Compressive strength. $^{*}p < 0.05$ *vs* PEEK, $^{\#}p < 0.05$ *vs* 3%Ta-PEEK, $^{\Delta}p < 0.05$ *vs* 5%Ta-PEEK.

Table 2
TGA and DSC results.

Sample	Residue weight (%)	T_g (°C)	T_c (°C)	T_m (°C)	ΔCp (J/(g∗K))	H_m (J/g)	X_c (%)
PEEK	0	145.7	294.0	343.0	0.136	49.38	37.98
1%Ta-PEEK	0.9388	142.1	291.0	343.0	0.109	47.37	36.81
3%Ta-PEEK	3.1891	141.5	283.0	342.0	0.042	40.69	32.27
5%Ta-PEEK	5.2653	143.1	285.0	341.0	0.050	36.62	29.65
7%Ta-PEEK	7.4298	144.6	284.0	341.0	0.061	40.75	33.71
9%Ta-PEEK	9.5502	144.5	284.0	341.0	0.063	41.54	35.11

2.4. In vivo studies

2.4.1. Animal surgery

All the animal procedures and experiments were approved by the Animal Ethical Committee at the Tongji Hospital, Tongji Medical School, Huazhong University of Science and Technology. 12-week-old Sprague Dawley rats were used to create the rat femur model. All surgical procedures were conducted under sterile conditions (Laboratory Animal Center of Tongji Medical College of Huazhong University of Science and Technology). Briefly, the rats were anesthetized with sodium pentobarbital. After fixing the rat on the operation desk properly, an incision along the axis of the thigh about 10 mm long was made to open the joint capsule. A hole (2 mm in diameter) was then drilled through the intercondylar notch and the distal femoral metaphysis with the direction parallel to the long axis of the femur. Two kinds of implants (cylindrical sample I and II) were placed bilaterally. The wound was closed by suturing the joint capsule and skin attentively. All rats were raised with normal feed and maintained under specific pathogen free conditions (SPF level) for 8 weeks.

2.4.2. Micro-computer tomography

All the rats were sacrificed after 8 weeks. Joints with cylindrical sample I implanted were fixed in 4% paraformaldehyde after dissection. The fixed samples were then scanned using micro-CT (vivaCT40, Scanco Medical, Switzerland). The scanning parameters were set as at 70 kV and 114 μA with an integration time of 380 ms and a resolution of 20 μm. Afterward, images were generated and three-dimensional models were reconstructed. Snapshots were taken in coronal sections.

2.4.3. Histological analysis

After micro-CT scanning, the specimens were dehydrated and embedded in polymethylmethacrylate (PMMA) and performed hard tissue sectioning with a microtome (model SP1600, Leica Microsystems, Wetzlar, Germany). Van Gieson's picrofuchsin staining was then performed to visualize the tissue. Panoramic Images were taken under a light microscope using Multiple Image Alignment (MIA) process.

2.4.4. Shear strength

The other joints of the rats with cylindrical sample II were then immediately performed mechanical test after sacrificing and dissection in a fresh statement. The samples were fixed on the mechanical testing machine (3300 Floor Model Universal Testing Systems, Instron, USA) using special tools illustrated in Fig. 1C. The pull-out test was then performed on the specimen with a constant speed of 0.1 mm/s. The shear strength could be calculated using equations Eqs. (2) and (3).

$$\text{Shear strength} = \text{pull out force/contact area} \quad (2)$$

$$\text{Contact area of the sample} = 2\pi r \times l = 2\pi \times 1\text{mm} \times 10\text{mm} \quad (3)$$

2.5. Statistical analysis

All datasets were found to be parametric and normally distributed therefore were expressed as means ± standard deviation. Statistically significant differences among groups were analyzed using one-way ANOVA and Tukey's multiple comparison tests in SPSS12 (IBM SPSS. Armonk, NY 10540, U.S.A). Statistically significant differences were considered at $p < 0.05$.

3. Results and discussion

3.1. Material properties

3.1.1. Surface morphology and characteristics

The surfaces of pure PEEK and tantalum nanoparticles reinforced

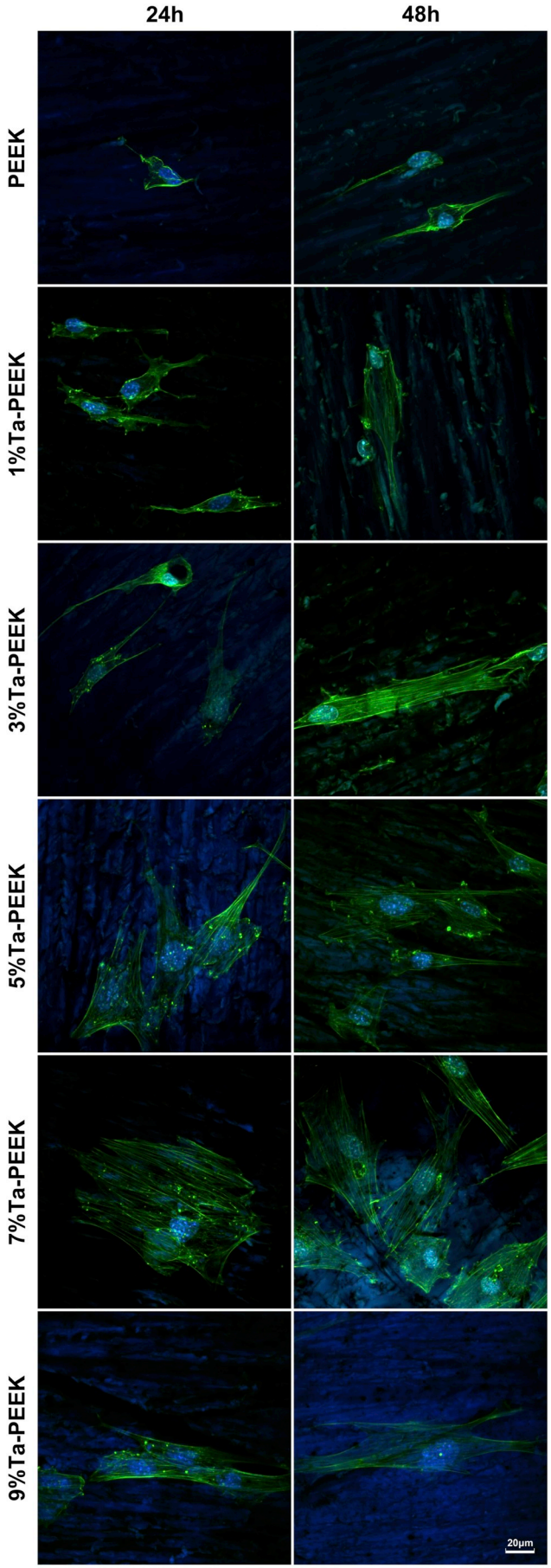

Fig. 4. Cell adhesion after 24 h and 48 h analyzed by confocal microscopy.

PEEK were shown in Fig. 2. It was shown that the tantalum nanoparticles were relatively evenly spread in the PEEK material. Although agglomeration could be observed in low resolution, which is often expected in using nanoparticles, images in high resolution indicated that the dispersion was uniform. To further prove the tantalum existence in the materials, EDS was performed. Results of EDS showed tantalum peaks and the quantification results were in accordance with the study design. On the other hand, the surface roughness had no difference among the groups which was proved by profilometers analysis. All the selected parameters - S_a, S_{ci}, S_{ku}, S_{sk}, showed no difference among the groups (Fig. 3A). Therefore, all the samples were normalized and thus only the tantalum content was the altering factor for the specimens.

3.1.2. Contact angles and mechanical properties

No significant difference was found in contact angles among the tested groups (Fig. 3C). Changed elastic modulus and compressive strength were observed after the addition of tantalum nanoparticles (Fig. 3D and E). Enhanced elastic modulus for the 1%Ta-PEEK, 3%Ta-PEEK and 5%Ta-PEEK samples were shown in the mechanical tests while enhanced compressive strength was shown in all the tantalum reinforced groups compared to PEEK. Highest enhanced mechanical properties were found in 3%Ta-PEEK. The elastic modulus and compressive strength decreased when the weight ratio of tantalum was higher than 3%.

Elastic modulus is one of the most important factors that can significantly influence the bone behavior on the biomaterials. Normally the elastic modulus of human bone ranges from 0.1 GPa to 18 GPa, depending on the location and type (cancellous or cortical) [36]. As is known to us that the high elastic modulus of metals can cause a stress shielding effect on the peri-implant bones, especially in load-bearing areas such as the femur, leading to the adsorption of adjacent bone tissues and causing prosthetic loosening [37]. Therefore, new methods were developed to lower the elastic modulus of metal implants such as increasing the porosity of metal materials. Porous tantalum scaffolds could provide an elastic modulus as low as 2.5 to 3.9 GPa [8]. Although good bone ingrowth was provided in porous form, however, the strength of implants would be sacrificed thus it is quite limited when used in high load-bearing positions as the compressive strength for such porous structures was reported to be 50–70 MPa [36]. In our research, Young's modulus of our materials was in the range of that of human bone tissue, and it could be adjusted according to the weight ratio of tantalum. On the other hand, generally the compressive strength was > 100 MPa, which was much higher than that of porous tantalum. Therefore, this kind of material is quite suitable for load-bearing area as high strength and comparable modulus are simultaneously needed. The elastic modulus and compressive strength increased as the content of tantalum in PEEK increased from 0 wt% to 3 wt%, but they began to decrease from 5 wt%. Thus 3%Ta-PEEK had the highest elastic modulus and compressive strength among all the groups, providing us with a good choice for mimicking the natural bone mechanical properties.

3.1.3. TGA and DSC tests

The TGA analysis showed corresponding results to the weight ratio of each group. For the DSC test, results indicated decreased crystallinity from 1%Ta-PEEK to 5%Ta-PEEK, while the crystallinity degree began to rise again when the content of tantalum was higher than 7 wt%. It was also interesting to notice that the T_g and T_c were lowest in 3%Ta-PEEK, and the addition of tantalum also altered T_m (Table 2 and Supplementary 2). Above all, the crystallinity structure was modified with the addition of tantalum and these thermal analysis results could partly explain the mechanical results where 3%Ta-PEEK and 5%Ta-PEEK exhibited preferable mechanical properties.

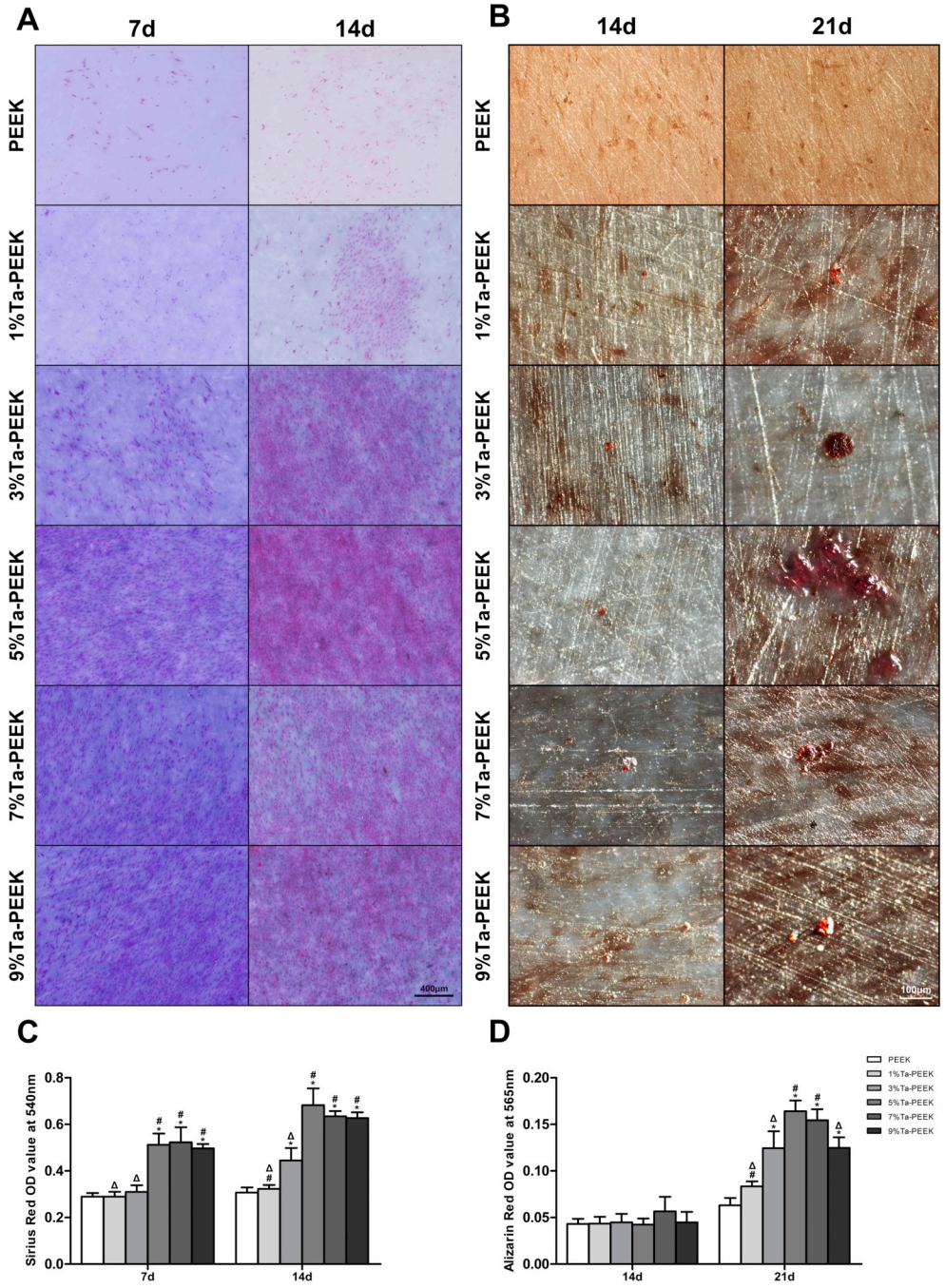

Fig. 5. Sirius red and Alizarin red staining results. (A) Images of Sirius red staining. (B) Images of Alizarin red staining. (C, D) Quantification of Sirius red and Alizarin red. $^{*}p < 0.05$ *vs* PEEK, $^{\#}p < 0.05$ *vs* 3%Ta-PEEK, $^{\Delta}p < 0.05$ *vs* 5%Ta-PEEK. (For interpretation of the references to colour in this figure legend, the reader is referred to the web version of this article.)

3.2. In vitro studies

3.2.1. Cell adhesion and toxicity

In order to investigate the biological effects of the composite, a series of *in vitro* experiments were conducted. MC3T3-E1 cell line, an osteoblast precursor cell line, is broadly used for testing bone formation related *in vitro* experiments. Although human osteoblasts might be a more optimal cell type when doing bone behavior related *in vitro* studies, the differences between donors might cause unstable results [38]. Instead, the cell line can provide stable and repeatable cell behavior and are quite suitable for preliminary investigations, thus MC3T3-E1 cells were chosen and seeded on the surface of our materials [39]. Cells behavior could be influenced by many factors. Toxicity and adhesion are of the most important initial behaviors that could influent the whole process afterward. Results showed no difference of LDH activity was found among the groups, and no toxic effects were observed in all groups (Fig. 6A). At 24 h, the cell morphology observed suggested that the cells spread relatively poorly onto the PEEK surfaces, exhibiting a spherical morphology, while cells on the surfaces of 5%Ta-PEEK and 7%Ta-PEEK materials had already extended well. Cells on the surfaces of 1%Ta-PEEK and 9%Ta-PEEK spread out but not fully extended. By 48 h, cells on the surface of PEEK and 1%Ta-PEEK were partly extended but not to the same degree as those on 5%Ta-PEEK and 7%Ta-PEEK (Fig. 4). Above all, adhesion of cells was improved on the surface of Ta-PEEK especially 5%Ta-PEEK and 7%Ta-PEEK. Since the surface roughness exhibited no difference among the groups, it could be

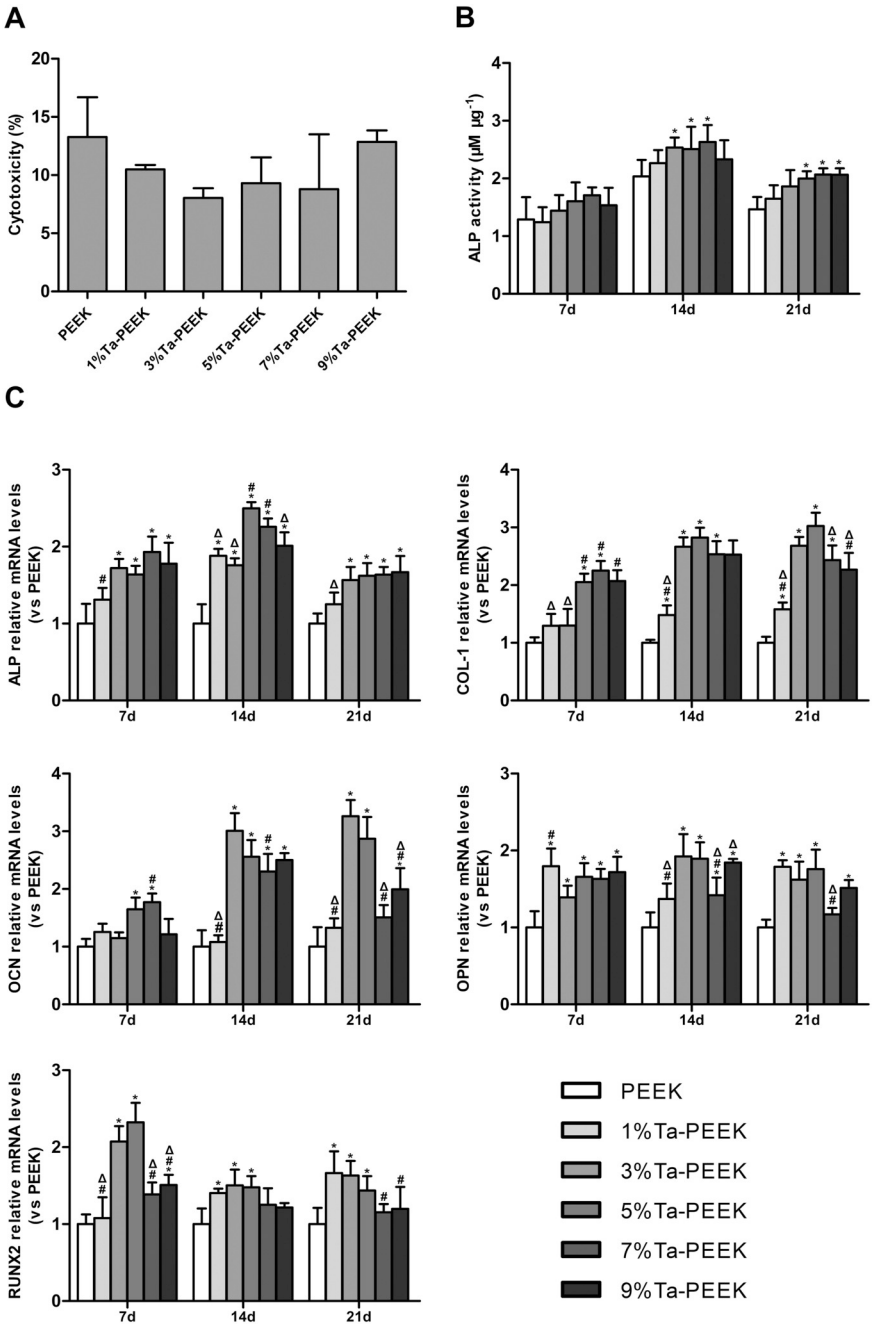

Fig. 6. Cytotoxicity, ALP activity and qPCR. (A) Cytotoxicity test *via* LDH activity analysis. No significant difference was found among the groups ($p > 0.05$). (B) ALP activity. (C) Osteogenesis related gene expression analyzed by qPCR. $^{*}p < 0.05$ *vs* PEEK, $^{\#}p < 0.05$ *vs* 3%Ta-PEEK, $^{\Delta}p < 0.05$ *vs* 5%Ta-PEEK.

deduced that the cell adhesion was enhanced by the materials themselves.

3.2.2. ALP activity

ALP activity was applied by measuring the ALP secretions in the culturing medium. Fig. 6B shows the quantitative ALP secretion of MC3T3-E1 cells on the samples. On the 7th day, difference of ALP activity was found by comparing 1%Ta-PEEK and 7%Ta-PEEK. No other differences were found in other comparisons. After 14 days, ALP difference was significantly higher when comparing 3%Ta-PEEK, 5%Ta-PEEK and 7%Ta-PEEK to pure PEEK. By the day 21, significant difference could still be found by comparing 5%Ta-PEEK, 7%Ta-PEEK and 9%Ta-PEEK to PEEK. Above all, the tantalum particles reinforced PEEK showed enhanced ALP activity.

3.2.3. Collagen secretion and biomineralization

Bone tissue has a complex structure of collagen fibers and mineralized calcium salt, which together provide both high level of strength and elasticity, making the bone possible to bear the load as well as the impact from different directions. It was found by Liisa et al. that crystal size in cortical bones was larger than cancellous bones, as well as the Ca/P ratio, while the residual protein content was much higher in cancellous bone [40]. Therefore, collagen secretion and extracellular mineralization are of the significant markers for bone formation.

Sirius red was used as the marker of collagen in this study. According to the images in Fig. 5A, it could be observed that more collagen was secreted on the surface of 3%Ta-PEEK, 5%Ta-PEEK, 7%Ta-PEEK and 9%Ta-PEEK after 7 days and 14 days. The quantification results were consistent to that of imaging. Significant differences

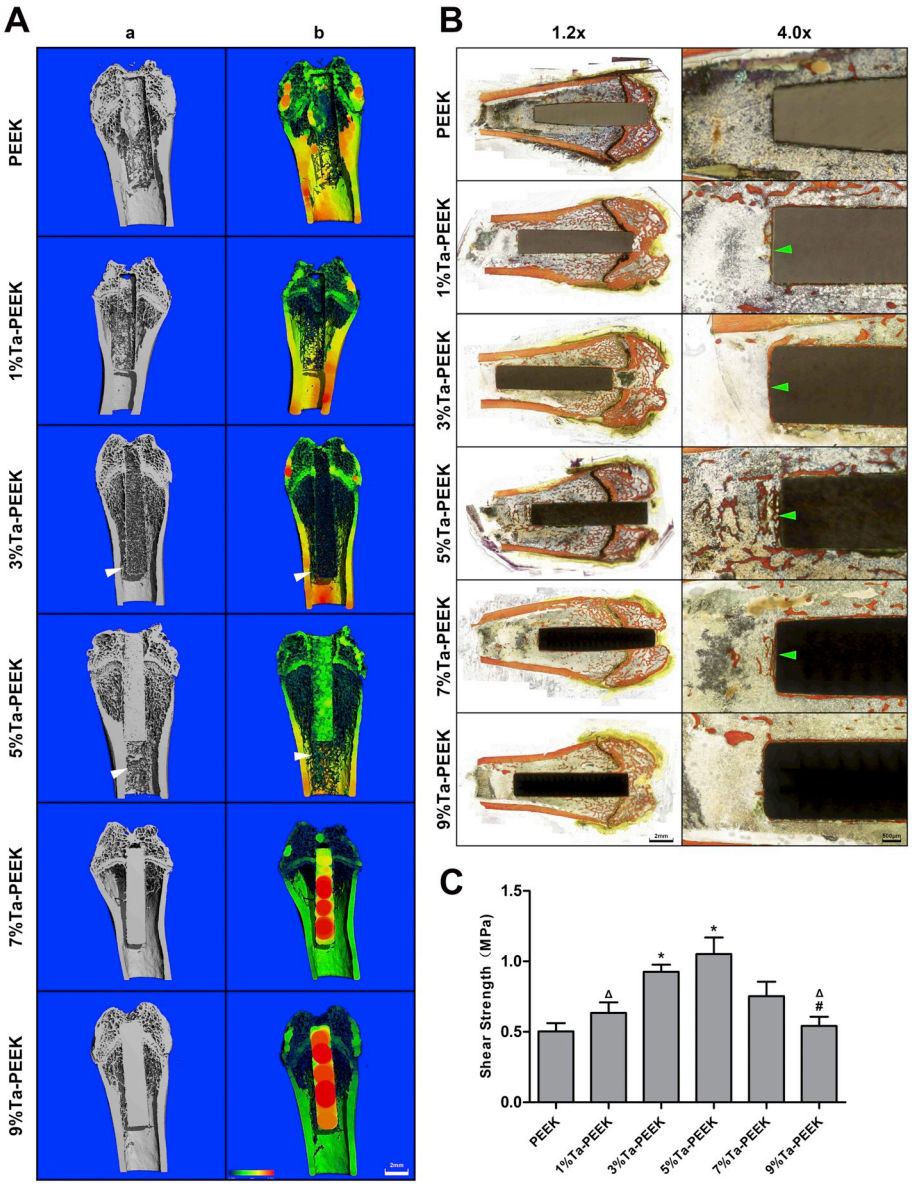

Fig. 7. Results of *in vivo* tests. (A) Sectional images of micro-CT reconstruction models. Images in column b were shown in density-spectrum scale. The enhanced new bone formation was shown on 3% and 5%Ta-PEEK (white arrows). (B) The histological result with Van Gieson's picrofuchsin staining. Images were shown in two magnifications. Green arrows referred to the newly formed bone on the implant surface. (C) Shear strength after 8 weeks. $^{*}p < 0.05$ *vs* PEEK, $^{\#}p < 0.05$ *vs* 3%Ta-PEEK, $^{\Delta}p < 0.05$ *vs* 5%Ta-PEEK. (For interpretation of the references to colour in this figure legend, the reader is referred to the web version of this article.)

were found by comparing 5%Ta-PEEK, 7%Ta-PEEK and 9%Ta-PEEK to pure PEEK respectively by two time points and also found by comparing 3%Ta-PEEK to PEEK by day 14 (Fig. 5C).

Extracellular matrix mineralization effects of MC3T3-E1 cells on the surface of the material were determined by Alizarin red staining. Results were shown in Fig. 5B. Small calcium nodes appeared on the surface of tantalum reinforced PEEK after 14 days and no calcified phenomenon were observed at this time point on the surface of PEEK. After 21 days, bone formation effects could be found in all groups but more and bigger calcified nodes could be seen on 3%Ta-PEEK, 5%Ta-PEEK and 7%Ta-PEEK compared to other groups. In quantitative analysis, no significant difference was found on the day 14 among the groups while the OD values of Alizarin red in 3%Ta-PEEK, 5%Ta-PEEK, 7%Ta-PEEK and 9%Ta-PEEK were significantly higher than that of PEEK after 3 weeks (Fig. 5D).

Extracellular matrix plays the key role in responding to the stiffness of the surface of the material. Engler et al. found that mesenchymal stem cells were able to specify the lineage and commit to certain phenotypes with extreme sensitivity to the matrix elasticity of tissue level [41]. Hence, it can be deduced that the surfaces characters including the elastic modulus of 3%Ta-PEEK and 5%Ta-PEEK were beneficial to osteogenic differentiation since they provide more similar elastic modulus to that of human cancellous bone. Cell study from Kang et al. demonstrated that tantalum nanoparticle could induce osteoblast proliferation with the involvement of autophagy [14]. It was also indicated that Ta–OH group could be formed on the surface when the tantalum material was soaked in a simulated body fluid, and the Ta–OH groups could combine with Ca^{2+} and phosphate ions to promote the apatite nucleation [42–44]. Therefore, the microenvironments of Ta-PEEK surface had a promoting effect for osteogenesis and more collagen fibrils and calcium nodes were then deposited and formed on the 5%Ta-PEEK surface. However, it was intriguing to notice that when the content of tantalum particles went higher, *e.g.* 7%Ta-PEEK and 9%Ta-PEEK, the osteogenesis effect did not go stronger. One possible explanation is the balance between the surface stiffness and tantalum content. Further experiments are needed to demonstrate the reason for

it.

3.2.4. Osteogenesis related gene expression

To investigate the differentiation effects of the composite, the expressions of typical osteogenesis-related genes were quantified by real-time PCR (Fig. 6C). All results were normalized to β-actin and shown as relative expression levels to the pure PEEK. Results in Fig. 6C showed that generally 3%Ta-PEEK, 5%Ta-PEEK and 7%Ta-PEEK exhibited better gene expression results. It was considered that COL-I and ALP were the early markers while OCN and OPN were markers that were usually highly expressed in later osteogenic differentiation stages. In our cases, generally the PEEK material with tantalum exhibited better gene expression levels for bone formation markers when compared to pure PEEK. PEEK with content of tantalum higher than 3% had the highest level of ALP after 14 days, while highly expressed OCN by day 14 and 21. 3%Ta-PEEK and 5%Ta-PEEK had significantly higher expression of OPN after 14 days and 21 days. The expression of COL-1 was high in 5%Ta-PEEK, 7%Ta-PEEK and 9%Ta-PEEK in all the three time points but 3%Ta-PEEK also exhibited preferable COL-1 expression by day 14 and 21. For RUNX2, 3%Ta-PEEK and 5%Ta-PEEK had the highest expression level on the 7th day. Therefore, MC3T3-E1 cells on the 3%Ta-PEEK and 5%Ta-PEEK surfaces exhibited stronger osteogenic differentiation tendency on the genetic levels in general as well.

3.3. In vivo studies

3.3.1. Micro-CT reconstruction

The potential of Ta-PEEK as an implant material was proved in our *in vivo* experiment. Fig. 7A shows the images captured in 3D models reconstructed after Micro-CT scanning. Coronal sections were applied to present the relations between material and bone in the femur condyles. Sectional images of the reconstructed models were shown in two different modes. The spectrum scale in Fig. 7Ab referred to the density. Since PEEK and 1%Ta-PEEK were relatively low in density, these two materials were not shown in the reconstruction models. It was obvious that enhanced new bone formation was shown on 3% and 5% Ta-PEEK, especially 5%Ta-PEEK (white arrows in Fig. 7A). It could also be observed that 3%Ta-PEEK presented similar density to spongy bone while 5%Ta-PEEK presented similar density to cortical bone.

3.3.2. Histological analysis

Histological sections with Van Gieson's staining were shown in Fig. 7B. Full views of the sample were shown by applying MIA. It could be observed that more new bones were formed around the 5%Ta-PEEK compared to other groups. On the other hand, fibrous tissues attached around the PEEK implant, separating the bone from contacting the surface of the material. For the other groups, new bone formation could be observed but they were not as thick as that of 5%Ta-PEEK. 5%Ta-PEEK exhibited obviously better osseointegration effect compared to other groups.

3.3.3. Osseointegration strength

Osseointegration strength was detected by measuring the shear strength of samples in femur after 8 weeks to further prove that the integration between the specimens and bones was intact and strong enough, which was shown in Fig. 7C. Obviously 5%Ta-PEEK and 3%Ta-PEEK had significantly higher integrating strength compared to pure PEEK. Statistical differences were also found when comparing 5%Ta-PEEK to 1%Ta-PEEK and 9%Ta-PEEK. These results were consistent with the histological result and Micro-CT results.

4. Conclusion

In the current study, tantalum nanoparticles were used to reinforce PEEK. The compressive strength and elastic modulus were increased for the 3%Ta-PEEK and 5%Ta-PEEK samples. The *in vitro* experiments showed preferable cell behaviors and osteogenesis effects in samples reinforced with tantalum nanoparticle. Enhanced bioactivity and promoted bone formation of 3%Ta-PEEK and 5%Ta-PEEK were also observed when compared to others groups for *in vivo* experiments, proved by higher pull-out forces along with histological evidence. This suggested that the addition of tantalum nanoparticles modified the osseointegration ability of PEEK. This composite of tantalum and PEEK could have a clinical potential for orthopedic implants.

Supplementary data to this article can be found online at https://doi.org/10.1016/j.msec.2019.03.091.

Acknowledgments

This work was supported by the National Natural Science Foundation of China [grant numbers 81572200 and 81772396]; the Norwegian Research Council [grant number 231530]; and the exchange project from China Scholarship Council and Norway Research Council.

References

[1] D.F. Williams, Biocompatibility pathways: biomaterials-induced sterile inflammation, mechanotransduction, and principles of biocompatibility control, ACS Biomater. Sci. Eng. 3 (2017) 2–35.
[2] A.J. Rahyussalim, A.F. Marsetio, I. Saleh, T. Kurniawati, Y. Whulanza, The needs of current implant technology in orthopaedic prosthesis biomaterials application to reduce prosthesis failure rate, J. Nanomater. 9 (2016), https://doi.org/10.1155/2016/5386924.
[3] M. Geetha, A.K. Singh, R. Asokamani, A.K. Gogia, Ti based biomaterials, the ultimate choice for orthopaedic implants - a review, Prog. Mater. Sci. 54 (2009) 397–425.
[4] E. Gibon, D.F. Amanatullah, F. Loi, J. Pajarinen, A. Nabeshima, Z.Y. Yao, M. Hamadouche, S.B. Goodman, The biological response to orthopaedic implants for joint replacement: part I: metals, J. Biomed. Mater. Res. B Appl. Biomater. 105 (2017) 2162–2173.
[5] G. Ryan, A. Pandit, D.P. Apatsidis, Fabrication methods of porous metals for use in orthopaedic applications, Biomaterials 27 (2006) 2651–2670.
[6] M. Niinomi, M. Nakai, J. Hieda, Development of new metallic alloys for biomedical applications, Acta Biomater. 8 (2012) 3888–3903.
[7] J.W. Lee, H.B. Wen, P. Gubbi, G.E. Romanos, New bone formation and trabecular bone microarchitecture of highly porous tantalum compared to titanium implant threads: a pilot canine study, Clin. Oral Implants Res. 29 (2018) 164–174.
[8] B.R. Levine, S. Sporer, R.A. Poggie, C.J. Della Valle, J.J. Jacobs, Experimental and clinical performance of porous tantalum in orthopedic surgery, Biomaterials 27 (2006) 4671–4681.
[9] J.A. Hanzlik, J.S. Day, G. Acknowledged Contributors: Ingrowth Retrieval Study, Bone ingrowth in well-fixed retrieved porous tantalum implants, J. Arthroplast. 28 (2013) 922–927.
[10] Y. Nakashima, N. Mashima, H. Imai, N. Mitsugi, N. Taki, Y. Mochida, I. Owan, K. Arakaki, T. Yamamoto, T. Mawatari, G. Motomura, M. Ohishi, T. Doi, M. Kanazawa, Y. Iwamoto, Clinical and radiographic evaluation of total hip arthroplasties using porous tantalum modular acetabular components: 5-year follow-up of clinical trial, Mod. Rheumatol. 23 (2013) 112–118.
[11] I. De Martino, V. De Santis, P.K. Sculco, R. D'Apolito, L.A. Poultsides, G. Gasparini, Long-term clinical and radiographic outcomes of porous tantalum monoblock acetabular component in primary hip arthroplasty: a minimum of 15-year follow-up, J. Arthroplast. 31 (2016) S110–S114.
[12] G. Mohandas, N. Oskolkov, M.T. McMahon, P. Walczak, M. Janowski, Porous tantalum and tantalum oxide nanoparticles for regenerative medicine, Acta Neurobiol. Exp. 74 (2014) 188–196.
[13] Q. Wang, H. Zhang, Q.J. Li, L. Ye, H.Q. Gan, Y.J. Liu, H. Wang, Z.Q. Wang, Biocompatibility and osteogenic properties of porous tantalum, Exp. Ther. Med. 9 (2015) 780–786.
[14] C.R. Kang, L.M. Wei, B. Song, L.J. Chen, J. Liu, B. Deng, X. Pan, L.Q. Shao, Involvement of autophagy in tantalum nanoparticle-induced osteoblast proliferation, Int. J. Nanomedicine 12 (2017) 4323–4333.
[15] S.M. Kurtz, J.N. Devine, PEEK biomaterials in trauma, orthopedic, and spinal implants, Biomaterials 28 (2007) 4845–4869.
[16] M.G. Wiesli, M. Ozcan, High-performance polymers and their potential application as medical and oral implant materials: a review, Implant. Dent. 24 (2015) 448–457.
[17] N.J. Hallab, K. McAllister, M. Brady, M. Jarman-Smith, Macrophage reactivity to different polymers demonstrates particle size- and material-specific reactivity: PEEK-OPTIMA((R)) particles versus UHMWPE particles in the submicron, micron, and 10 micron size ranges, J Biomed Mater Res B Appl Biomater 100 (2012) 480–492.
[18] S. Utzschneider, F. Becker, T.M. Grupp, B. Sievers, A. Paulus, O. Gottschalk, V. Jansson, Inflammatory response against different carbon fiber-reinforced PEEK wear particles compared with UHMWPE in vivo, Acta Biomater. 6 (2010) 4296–4304.
[19] K.B. Sagomonyants, M.L. Jarman-Smith, J.N. Devine, M.S. Aronow, G.A. Gronowicz, The in vitro response of human osteoblasts to

polyetheretherketone (PEEK) substrates compared to commercially pure titanium, Biomaterials 29 (2008) 1563–1572.
[20] J.M. Toth, M. Wang, B.T. Estes, J.L. Scifert, H.B. Seim, A.S. Turner, Polyetheretherketone as a biomaterial for spinal applications, Biomaterials 27 (2006) 324–334.
[21] R. Ma, T. Tang, Current strategies to improve the bioactivity of PEEK, Int. J. Mol. Sci. 15 (2014) 5426–5445.
[22] D. Garcia-Gonzalez, M. Rodriguez-Millan, A. Rusinek, A. Arias, Investigation of mechanical impact behavior of short carbon-fiber-reinforced PEEK composites, Compos. Struct. 133 (2015) 1116–1126.
[23] C.S. Li, C. Vannabouathong, S. Sprague, M. Bhandari, The use of carbon-fiber-reinforced (CFR) PEEK material in orthopedic implants: a systematic review, Clin. Med. Insights Arthritis Musculoskelet. Disord. 8 (2015) 33–45.
[24] I. Nakahara, M. Takao, S. Bandoh, N. Bertollo, W.R. Walsh, N. Sugano, In vivo implant fixation of carbon fiber-reinforced PEEK hip prostheses in an ovine model, J. Orthop. Res. 31 (2013) 485–492.
[25] I. Nakahara, M. Takao, T. Goto, C. Ohtsuki, S. Hibino, N. Sugano, Interfacial shear strength of bioactive-coated carbon fiber reinforced polyetheretherketone after in vivo implantation, J. Orthop. Res. 30 (2012) 1618–1625.
[26] Y. Deng, X.C. Liu, A.X. Xu, L.X. Wang, Z.Y. Luo, Y.F. Zheng, F. Deng, J. Wei, Z.H. Tang, S.C. Wei, Effect of surface roughness on osteogenesis in vitro and osseointegration in vivo of carbon fiber-reinforced polyetheretherketone-nanohydroxyapatite composite, Int. J. Nanomedicine 10 (2015) 1425–1447.
[27] Y.S. Pan, Y. Chen, Q.Q. Shen, Flexural mechanical properties of functional gradient hydroxyapatite reinforced polyetheretherketone biocomposites, J. Mater. Sci. Technol. 32 (2016) 34–40.
[28] T. Lu, J. Wen, S. Qian, H.L. Cao, C.Q. Ning, X.X. Pan, X.Q. Jiang, X.Y. Liu, P.K. Chu, Enhanced osteointegration on tantalum-implanted polyetheretherketone surface with bone-like elastic modulus, Biomaterials 51 (2015) 173–183.
[29] F. Suska, O. Omar, L. Emanuelsson, M. Taylor, P. Gruner, A. Kinbrum, D. Hunt, T. Hunt, A. Taylor, A. Palmquist, Enhancement of CRF-PEEK osseointegration by plasma-sprayed hydroxyapatite: a rabbit model, J. Biomater. Appl. 29 (2014) 234–242.
[30] S.C. Scholes, A. Unsworth, Pitch-based carbon-fibre-reinforced poly (ether-ether-ketone) OPTIMA (R) assessed as a bearing material in a mobile bearing unicondylar knee joint, Proc. Inst. Mech. Eng. H J. Eng. Med. 223 (2009) 13–25.
[31] S.C. Scholes, A. Unsworth, Wear studies on the likely performance of CFR-PEEK/CoCrMo for use as artificial joint bearing materials, J. Mater. Sci. Mater. Med. 20 (2009) 163–170.
[32] M. Sumer, H. Unal, A. Mimaroglu, Evaluation of tribological behaviour of PEEK and glass fibre reinforced PEEK composite under dry sliding and water lubricated conditions, Wear 265 (2008) 1061–1065.
[33] C.L. Brockett, G. John, S. Williams, Z. Jin, G.H. Isaac, J. Fisher, Wear of ceramic-on-carbon fiber-reinforced poly-ether ether ketone hip replacements, J Biomed Mater Res B Appl Biomater 100 (2012) 1459–1465.
[34] Q.H. Wang, Q.J. Xue, W.C. Shen, J.Y. Zhang, The friction and wear properties of nanometer ZrO_2-filled polyetheretherketone, J. Appl. Polym. Sci. 69 (1998) 135–141.
[35] D.J.B.B.N. Osborn, The morphology of poly(aryl-ether-ether-ketone), Polymer 24 (1983) 953.
[36] Y.D. Liu, C.Y. Bao, D. Wismeijer, G. Wu, The physicochemical/biological properties of porous tantalum and the potential surface modification techniques to improve its clinical application in dental implantology, Mater. Sci. Eng. C Mater. Biol. Appl. 49 (2015) 323–329.
[37] Z.N. Wan, L.D. Dorr, T. Woodstone, A. Ranawat, M. Song, Effect of stem stiffness and bone stiffness on bone remodeling in cemented total hip replacement, J. Arthroplast. 14 (1999) 149–158.
[38] C. NeidlingerWilke, I. Stalla, L. Claes, R. Brand, I. Hoellen, S. Rubenacker, M. Arand, L. Kinzl, Human osteoblasts from younger normal and osteoporotic donors show differences in proliferation and T-GF beta-release in response to cyclic strain, J. Biomech. 28 (1995) 1411–1418.
[39] W.N. Addison, V. Nelea, F. Chicatun, Y.C. Chien, N. Tran-Khanh, M.D. Buschmann, S.N. Nazhat, M.T. Kaartinen, H. Vali, M.M. Tecklenburg, R.T. Franceschi, M.D. McKee, Extracellular matrix mineralization in murine MC3T3-E1 osteoblast cultures: an ultrastructural, compositional and comparative analysis with mouse bone, Bone 71 (2015) 244–256.
[40] L.T. Kuhn, M.D. Grynpas, C.C. Rey, Y. Wu, J.L. Ackerman, M.J. Glimcher, A comparison of the physical and chemical differences between cancellous and cortical bovine bone mineral at two ages, Calcif. Tissue Int. 83 (2008) 146–154.
[41] A.J. Engler, S. Sen, H.L. Sweeney, D.E. Discher, Matrix elasticity directs stem cell lineage specification, Cell 126 (2006) 677–689.
[42] T. Miyazaki, H.M. Kim, T. Kokubo, C. Ohtsuki, H. Kato, T. Nakamura, Mechanism of bonelike apatite formation on bioactive tantalum metal in a simulated body fluid, Biomaterials 23 (2002) 827–832.
[43] T. Miyazaki, Development of bioactive materials based on bone-bonding mechanism on metal oxides, J. Ceram. Soc. Jpn. 116 (2008) 260–264.
[44] T. Kokubo, H.M. Kim, M. Kawashita, Novel bioactive materials with different mechanical properties, Biomaterials 24 (2003) 2161–2175.